Investigation of the Electronic Transport Properties of Nanocrystalline Particulate TiO_2 Electrodes by Intensity-Modulated Photocurrent Spectroscopy

P. E. de Jongh and D. Vanmaekelbergh*,†

Debye Institute, Utrecht University, 3508 TA Utrecht, The Netherlands

Received: July 23, 1996; In Final Form: November 4, 1996[⊗]

The transport of photogenerated electrons through nanocrystalline particulate TiO_2 electrodes has been investigated by intensity modulated photocurrent spectroscopy, using UV light for electron−hole pair generation. The optoelectrical admittance has been compared with that obtained with nanoporous crystalline GaP electrodes in which the transport of electrons through the porous network is simply diffusive. It is found that transport of photogenerated electrons through particulate TiO_2 electrodes is limited by trapping/detrapping in band gap states distributed in energy. It is argued that the electron traps are located at the TiO_2/electrolyte interface.

Introduction

The remarkable optoelectrical properties of macroscopic assemblies of semiconductor particles with dimensions in the nanometer range have attracted considerable scientific interest.[1−18] For instance, ordered, close-packed assemblies of quantized CdSe particles have been synthesized, and electronic energy transfer between the particles has been demonstrated.[1,2] A particulate assembly, in which the individual particles are electronically connected and which is provided with a contact to a metallic conductor, can be used as a particulate electrode. Particulate electrodes are promising for several optoelectrical applications. WO_3 electrodes show a very fast and efficient electrochromic action.[10] Solar cells based on particulate electrodes have remarkably high photocurrent quantum yields. Grätzel has proposed a cheap and highly efficient dye-sensitized TiO_2 solar cell, in which visible light is harvested by a monolayer of dye adsorbed on the internal surface of a porous TiO_2 electrode.[3] Electron−hole pairs are generated in the dye, but only the electron is transferred to the TiO_2, resulting in effective electron−hole pair separation. Reasonable high photocurrent quantum yields were also observed with CdSe and CdS electrodes consisting of 4−6 nm particles.[5] Nanoporous GaP and SiC electrodes show a huge enhancement of the photocurrent quantum yield for light absorbed in the indirect transition and sub-band-gap light with respect to electrodes with a flat geometry.[11−13] Charge separation is achieved due to the interpenetration of semiconductor and electrolyte on a nanometer scale; in this way, minority carriers are generated within a distance from the electrolyte smaller than the diffusion length.

The performance of a particulate electrode depends strongly on the electronic transport properties. Preliminary work with particulate TiO_2 and ZnO electrodes reported photocurrent and photovoltage transients with typical times in the millisecond to second range, indicating that the transport through particulate electrodes can be very slow.[7−9] Due to such a slow transport, back transfer of electrons into the electrolyte can occur, which is believed to be one of the recombination mechanisms in TiO_2-based solar cells.[6]

There are several reasons why the electronic transport properties of nanocrystalline particulate electrodes can considerably differ from those of single-crystalline electrodes. First, distortion of the crystal structure at grain boundaries may lead to enhanced scattering of electrons with the lattice, and hence to a reduced electron mobility. Localized states may be present at grain boundaries acting as electron traps. Second, particulate electrodes are highly porous networks in which solid and electrolyte are interpenetrated on a nanometer scale. As a result, electronic transport may be strongly influenced by the interfacial properties. For instance, free charge carriers can be trapped in surface states during their transport through the porous network.

In this study, electronic transport in nanocrystalline TiO_2 electrodes was investigated by intensity modulated photocurrent spectroscopy (IMPS). The electrode is illuminated with monochromatic light of energy exceeding the band gap: the light intensity consists of a background component Φ and a small amplitude sinusoidal modulation $\Phi(\omega)$. This gives rise to a steady state photocurrent density Δi and a photocurrent density response $\Delta i(\omega)$, harmonically varying with the same frequency as $\Phi(\omega)$. The steady state photocurrent quantum yield is $\Delta i/e\Phi$. The complex number $\Delta i(\omega)/e\Phi(\omega)$ has been called optoelectrical admittance. It can be represented in the complex plane with ω as a parameter. If the *RC* time of the porous electrode is shorter than the transit time of the photogenerated charge carriers through the porous network, the externally measured photocurrent response $\Delta i(\omega)$ corresponds to the internal photocurrent flow in the porous electrode which is due to the motion of charge carriers. In such a case, the transit time of photogenerated charge carriers through the porous network can be obtained from the optoelectrical admittance. This has been shown in a previous paper with single-crystalline nanoporous GaP electrodes.[14] The IMPS method presented here has some similarities with time of flight and photocurrent transient measurements.[15,16] However, with IMPS, steady state conditions are perturbed only by a small amplitude light intensity. This enables study of electronic transport under steady state conditions for the photocurrent flow and occupation of electronic states. This is important when trapping of charge carriers plays a role.[15]

The work with nanoporous GaP networks[14] will form a basis for understanding the results with nanocrystalline particulate TiO_2 electrodes. The main results and interpretation are therefore reconsidered here. Porous GaP films with a thickness between 1 and 200 μm were prepared by anodic etching of crystalline substrates under dielectric breakdown conditions.[11,12] The porous network consists of strongly interconnected struc-

† E-mail: D.Vanmaekelbergh@fys.ruu.nl.

[⊗] Abstract published in *Advance ACS Abstracts,* March 1, 1997.

S1089-5647(96)02226-2 CCC: $14.00

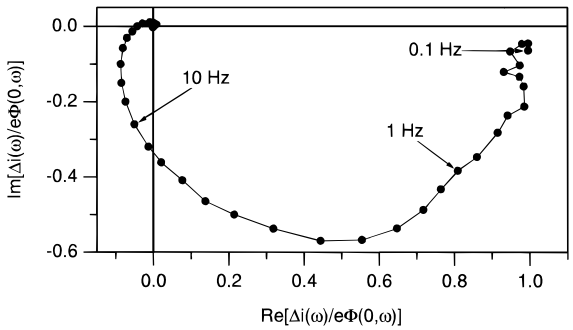

Figure 1. Complex plane representation of the optoelectrical admittance measured with a nanoporous GaP photoanode of 200 μm in thickness under conditions of severe depletion. Electrolyte is 1 M H_2SO_4.

tural units with dimensions of about 50−300 nm. A potential difference between the interior and surface of each unit leads to effective electron−hole pair separation. The holes migrate to the surface of the units and are transferred to the electrolyte which is interpenetrated in the GaP network. The steady state photocurrent quantum yield is one. The photogenerated electrons, withdrawn from the surface, travel through the porous structure toward the substrate. A representative plot of the optoelectrical admittance in the complex plane is given in Figure 1. Typically, a distorted semicircle is found, mainly located in the positive−negative quadrant. The low-frequency limit of $\Delta i(\omega)/e\Phi(\omega)$ is one. At a characteristic frequency, further denoted as ω_{min}, the imaginary component has a minimum value. At frequencies above ω_{min}, the plot shifts to the negative−negative quadrant, and finally,$\Delta i(\omega)/e\Phi(\omega)$ tends to zero. It was found that $1/\omega_{min}$ is independent of the background light intensity and proportional to the square of the thickness of the porous network. These results could be understood quantitatively on the basis of a model which assumes that photogenerated electrons drift through the porous GaP without being trapped. The continuity equation for the photogenerated electrons, with concentration $\Delta n(x,t)$, then reads

$$\mathrm{d}\Delta n(x,t)/\mathrm{d}t = \alpha\Phi(x,t) - \mathrm{d}\Delta j_n(x,t)/\mathrm{d}x \qquad (1)$$

In the above equation, $\alpha\Phi(x,t)$ is the photogeneration rate of the electrons, and $\Delta j_n(x,t)$ is the electron flux given by

$$\Delta j_n(x,t) = \mu_n \epsilon \Delta n(x,t) \qquad (2)$$

The driving force ϵ for the flow of photogenerated electrons is the gradient of the quasi-Fermi level, $\epsilon = (1/e)(\mathrm{d}E_{F,n}/\mathrm{d}x)$. It was assumed that ϵ is independent of x so that

$$\mathrm{d}\Delta j_n(x,t)/\mathrm{d}x = \mu_n \epsilon [\mathrm{d}\Delta n(x,t)/\mathrm{d}x] \qquad (3)$$

If $\Phi(x,t)$ varies harmonically with time with a frequency ω, $\Delta n(x,\omega)$ can be calculated by combining eqs 1 and 3. In this calculation, it was assumed that the driving force is not changed by modulation of the light intensity. The contribution of the electron motion to the optoelectrical admittance could then be calculated using

$$\Delta i_n(\omega) = (e/d)\mu_n(-\epsilon)\int_0^d \Delta n(x,\omega)\,\mathrm{d}x \qquad (4)$$

As the GaP electrode was illuminated through the electrolyte and the absorption depth ($1/\alpha$) of the UV light was much smaller than the thickness of the porous layer d, $\Delta i_n(\omega)$ approaches the total photocurrent response. For $\alpha d \gg 1$, it was found that the optoelectrical admittance is given by

$$i_n(\omega)/e\Phi(0,\omega) = [1 - \exp(-i\omega\tau_d)]/i\omega\tau_d \qquad (5)$$

Equation 5 is in accordance with the particular shape of the optoelectrical admittance which was found to shift from the positive−negative to the negative−negative quadrant in the frequency region above ω_{min}. τ_d is the transit time of the photogenerated electrons through the porous layer. It follows that τ_d can be obtained from the optoelectrical admittance plot:

$$\tau_d = d/\mu_e\,|\epsilon| = 2.5/\omega_{min} \qquad (6)$$

The driving force ϵ may have an electric field and a diffusive component. In both cases, it is reasonable to assume that ϵ is proportional to $1/d$ which makes τ_d proportional to d^2, in agreement with the experimental results.[14] The above model, involving simple diffusive transport of photogenerated charge carriers through a porous network, will be used as a basis for interpretation of the more complex results obtained with nanocrystalline TiO_2 electrodes.

Experimental Section

Particulate TiO_2 electrodes were prepared by dip-coating transparent conducting substrates in an aqueous TiO_2 suspension. The TiO_2 particles (Degussa P25) consisted of 75% anatase and 25% rutile, and the average size was 30 nm. The electrodes were sintered for 2 h at 450 °C under air to ensure electrical contact between the particles. The thickness of the electrodes as determined using a Tencor Alpha Step 500 surface profiler was 0.3, 0.9, and 4.0 μm; the geometrical surface area was 0.5 cm^2. The porosity of the electrodes was approximately 50%. Figure 2 shows a representative photograph of a 0.9 μm TiO_2 electrode, obtained with a Philips XL30 scanning electron microscope. It is clear that the dimensions of the individual particles are retained in the sintered three-dimensional network.

IMPS measurements were carried out using a PAR 273A potentiostat and a Solartron 1250 frequency response analyzer (FRA). The TiO_2 electrode served as working electrode in a standard three-electrode cell with a large platinum counter electrode and a saturated calomel electrode as a reference. The electrolyte was an aqueous 0.5 M Na_2SO_4 solution, which was purged with nitrogen before the measurements. The 354 nm line of an Ar ion laser (Coherent Innova) was used for electron−hole pair generation. About 20% of the background intensity was sinusoidally modulated using an Isomet 1211 acoustooptic modulator controlled by the FRA. A beam splitter and a fast silicon photodiode were used for measurement of the background and harmonically varying light intensity. The beam was expanded using a Newport beam expander to a spot diameter of 2 cm incident on the TiO_2 electrode.

Results

The photocurrent quantum yield $\Delta i/e\Phi$ measured with a 0.9 μm thick particulate TiO_2 electrode (illuminated through the Na_2SO_4 electrolyte) is shown as a function of the applied potential in Figure 3 (lower curve). The photocurrent quantum yield was virtually independent of the applied potential in the potential range more positive than −0.3 V. The quantum yield decreased with increasing light intensity (see further Figure 6). Typical values for our TiO_2 electrodes in Na_2SO_4 electrolyte were between 0.01 and 0.1. This shows that, in contrast to nanoporous GaP photoanodes, electron−hole pair separation is not fully effective. The photogenerated holes can either be transferred to the electrolyte (oxidation of water) or recombine with an electron. Recombination can be suppressed by adding an additional hole scavenger to the electrolyte.[17] This is

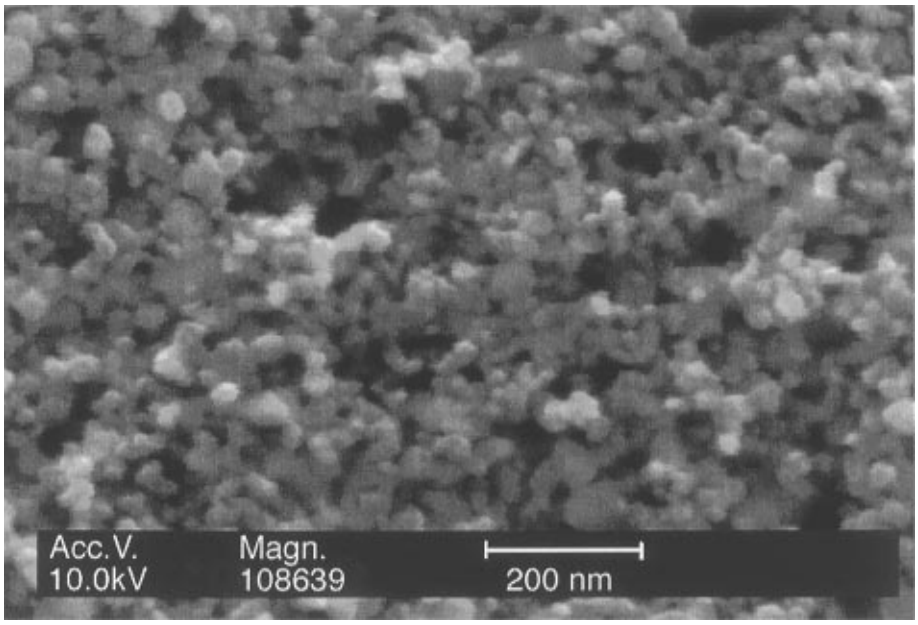

Figure 2. SEM photograph of a TiO_2 particulate network, prepared by dip-coating a conducting glass in a suspension of Degussa P25 particles and mild sintering at 450 °C.

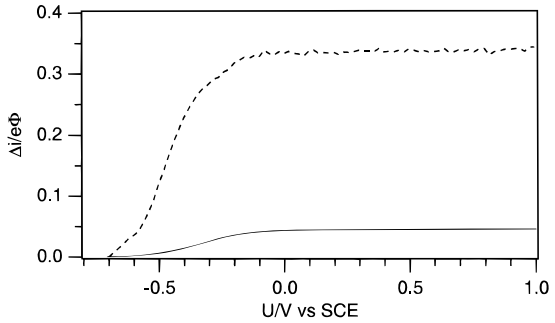

Figure 3. Plot of the steady state photocurrent quantum yield $\Delta i/e\Phi$ of a particulate TiO_2 electrode (thickness is 0.9 μm) as a function of the applied potential. The electrode is illuminated with UV light through the electrolyte; the absorbed light intensity Φ is 4.4 10^{15} cm^{-2} s^{-1}: Lower curve, electrolyte is 0.5 M Na_2SO_4 + H_2O; upper curve, after addition of 2.5 M MeOH.

illustrated in Figure 3: addition of 2.5 M methanol increases the photocurrent quantum yield markedly (upper curve).

In Figure 4, parts a−c, the optoelectrical admittance, $\Delta i(\omega)/e\Phi(\omega)$, measured with particulate TiO_2 electrodes of 0.3, 0.9, and 4.0 μm in thickness, illuminated via the electrolyte, is presented in the complex plane. The thickness of 0.3 μm corresponds approximately to the absorption depth of the 354 nm light. The plots are mainly located in the positive−negative quadrant, but shift into the negative−negative quadrant at higher frequencies, as was found with porous GaP electrodes (see Figure 1). At low frequencies, a point on the real axis is obtained corresponding to the steady state photocurrent quantum yield $\Delta i/e\Phi$. The dependence of $\Delta i/e\Phi$ on the background light intensity will be discussed later. At sufficiently high frequencies, $\Delta i(\omega)/e\Phi(\omega)$ approaches (0,0). The inverse of the frequency at which the imaginary component shows a minimum ω_{min} is a measure for the transit time of the photogenerated electrons. It was found that the transit time increases with increasing electrode thickness, but the dependence is not as strong as that measured with porous GaP electrodes for which $1/\omega_{min} \approx d^2$.[14] Figure 4, part d, shows a plot of the optoelectrical admittance of a 4.0 μm thick TiO_2 electrode which is illuminated through the transparent substrate. Two time constants are reflected in the plot. The small semicircle at lower frequencies has a characteristic frequency (about 10 s^{-1}) which is independent of the background light intensity. The larger semicircle has a characteristic frequency which increases markedly with the background light intensity, as for illumination via the electrolyte side. This semicircle hence reflects the transport of electrons through the particulate network. The transit time is much shorter than that for the same electrode illuminated from the electrolyte side and is comparable to that measured for the 0.3 μm thick electrode illuminated through the electrolyte.

It was found that, for a given electrode, ω_{min} depends strongly on the background light intensity. At very low light intensities, the transit times were orders of magnitude longer than at high light intensities. This is in sharp contrast to the results with nanoporous GaP, for which ω_{min} was found to be independent of the light intensity. From Figure 5, parts a−c, it is clear that ω_{min} is proportional to $\sqrt{\Phi}$ for all TiO_2 electrodes in Na_2SO_4 electrolyte, illuminated from the electrolyte side. Figure 5, part d, presents a plot of ω_m vs $\sqrt{\Phi}$ for a 0.9 μm thick electrode illuminated from the electrolyte side with 2.5 M methanol added to the electrolyte to enhance the photocurrent quantum yield. In this case, ω_{min} is also proportional to $\sqrt{\Phi}$, the proportionality constant being the half of that observed without methanol. Figure 5, part e, presents ω_{min} as a function of $\sqrt{\Phi}$ for a 0.9 μm thick TiO_2 electrode, measured in 1 M NaOH. The steady state photocurrent quantum yield in this electrolyte is comparable to that in Na_2SO_4 electrolyte. It can be seen that the ω_{min} vs $\sqrt{\Phi}$ plot is similar to that in Na_2SO_4 electrolyte.

The steady state photocurrent quantum yield $\Delta i/e\Phi$ decreased with increasing light intensity. In Figure 6, parts a and b, the low-frequency limit of the optoelectrical admittance is shown vs $1/\sqrt{\Phi}$ for the electrodes with a thickness of 0.9 and 4.0 μm in aqueous Na_2SO_4 electrolyte. It is clear that, at sufficiently high light intensity, $\Delta i/e\Phi$ is proportional to $1/\sqrt{\Phi}$.

Discussion

The photocurrent quantum yield for particulate TiO_2 electrodes, lying between 0.01 and 0.1, shows that photogenerated holes are consumed in two competitive processes: hole transfer to the electrolyte and electron−hole recombination. As charge carriers, photogenerated in a nanometer-sized particle, are readily trapped in surface states,[18] it will be assumed that the competition between recombination and charge transfer involves a

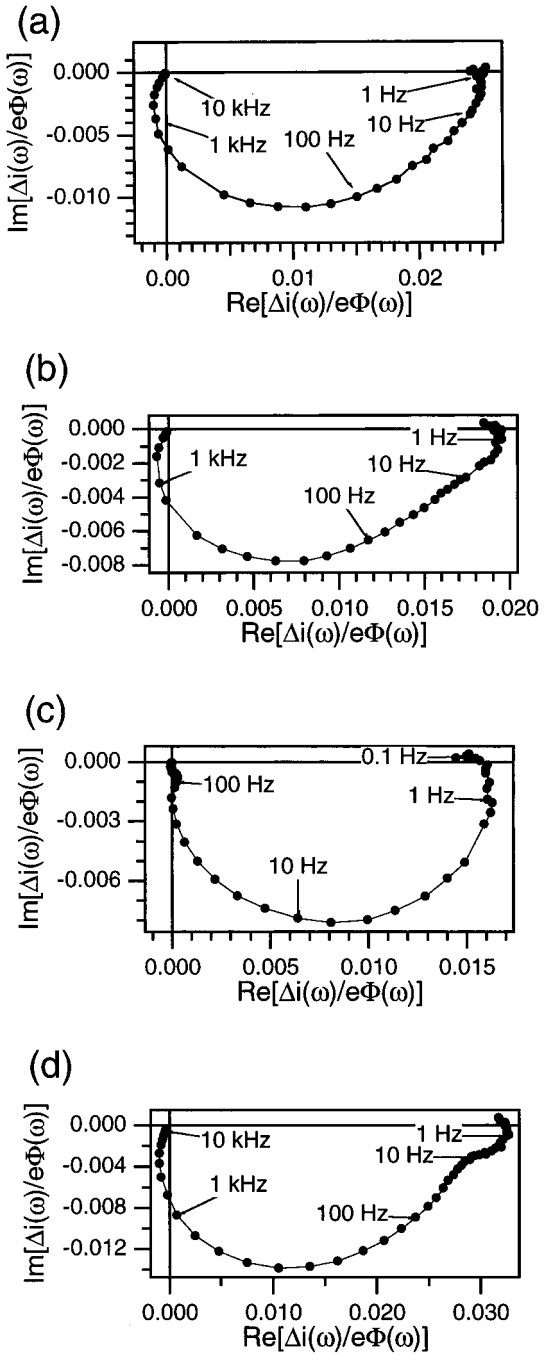

Figure 4. Complex plane representation of the optoelectrical admittance measured with particulate TiO_2 electrodes of different thicknesses d. The UV light is incident through the electrolyte, except for Figure 4, part d: (a) $d = 0.3$ μm, $\Phi = 1.2\ 10^{16}$ cm^{-2} s^{-1}; (b) $d = 0.9$ μm, $\Phi = 1.5\ 10^{16}$ cm^{-2} s^{-1}; (c) $d = 4.0$ μm, $\Phi = 2.1\ 10^{16}$ cm^{-2} s^{-1}; (d) $d = 4.0$ μm, $\Phi = 2.1\ 10^{16}$ cm^{-2} s^{-1}, illumination through the substrate.

surface-trapped hole as a common intermediate. In contrast to nanoporous GaP electrodes, the characteristic frequency of the optoelectrical admittance of particulate TiO_2 electrodes was found to depend on the background light intensity. This strongly suggests that electrons are temporarily localized in band gap states during their passage through the network. It will be assumed here that the states involved in trapping/detrapping are different from those which act as recombination centers. It is clear that the model of diffusive transport, accounting for the results obtained with porous GaP, must be extended to incorporate electron−hole recombination and trapping/detrapping of electrons.

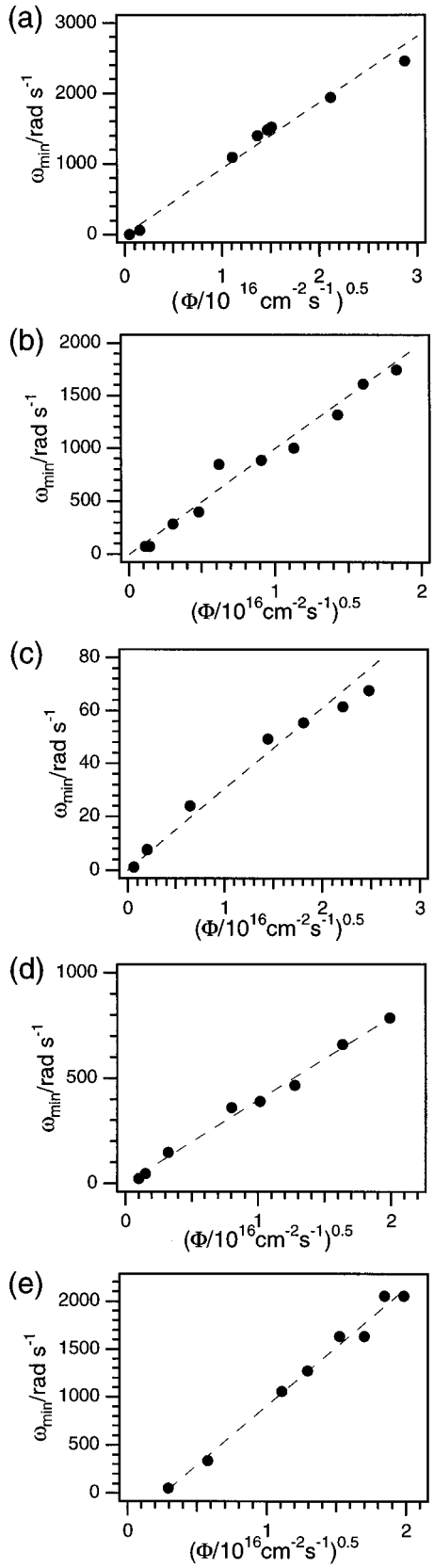

Figure 5. Plots of ω_{min} vs $(\Phi)^{1/2}$ measured under illumination through the electrolyte: (a) $d = 0.3$ μm, 0.5 M Na_2SO_4 + H_2O; (b) $d = 0.9$ μm, 0.5 M Na_2SO_4 + H_2O; (c) $d = 4.0$ μm, 0.5 M Na_2SO_4 + H_2O: (d) $d = 0.9$ μm, 0.5 M Na_2SO_4 + H_2O + 2.5 M MeOH; (e) $d = 0.9$ μm, 1 M NaOH + H_2O.

Figure 7 shows the essential features of a particulate TiO_2 electrode under illumination and anodic photocurrent flow. Photons, with energy exceeding the gap are absorbed leading

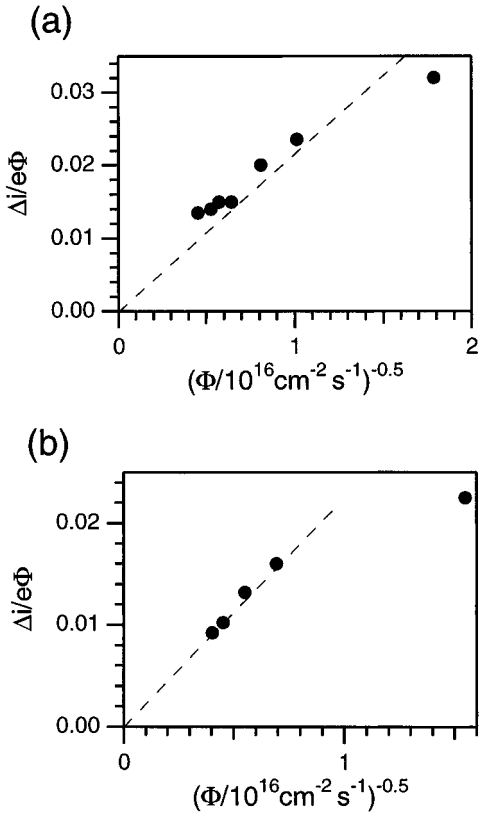

Figure 6. The low-frequency limit of the optoelectrical admittance as a function of $(\Phi)^{-1/2}$; the UV light is incident from the electrolyte side. The electrolyte is 0.5 M $Na_2SO_4 + H_2O$: (a) $d = 0.9$ μm; (b) $d = 4.0$ μm.

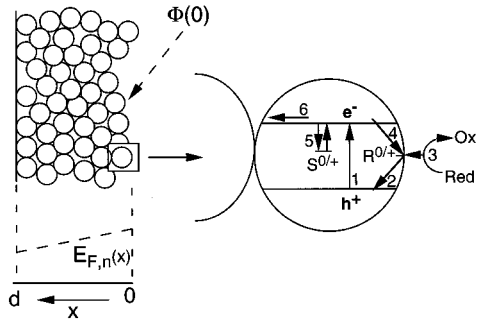

Figure 7. Sketch of a particulate TiO_2 electrode under illumination. The driving force for electron flow, $\epsilon = (dE_{F,n}/dx)$ is assumed to be independent of the spatial coordinate x. A scheme is also shown of the processes which are considered in the model (the arrows indicate electron transitions): (1) electron−hole pair generation; (2) trapping of holes in interfacial states $R^{0/+}$; (3) electrochemical transfer of surface-trapped holes to the electrolyte; (4) electron trapping in $R^{0/+}$ leading to recombination; (5) electron trapping in $S^{0/+}$ and thermal release; (6) electron drift toward the substrate.

to electrons and holes:

process 1 in Figure 7

$$h\nu \rightarrow e^- + h^+$$

The holes (concentration $\Delta p(x,t)$) are trapped in surface states $R^{0/+}$ (total concentration r, electron occupancy $f_R(x,t)$) of the particle in which they are generated:

process 2 in Figure 7

$$h^+ + R^0 \xrightarrow{\beta_p} R^+$$

The continuity equation for the photogenerated holes is

$$d\Delta p(x,t)/dt = \alpha\Phi(x,t) - (\beta_p r)\, f_R(x,t)\Delta p(x,t) \qquad (7)$$

Photogenerated holes do not contribute directly to the time-resolved photocurrent, as they are consumed in the particle in which they are generated and thus do not travel through the porous network. A surface-trapped hole can be transferred to the electrolyte leading to an oxidized species:

process 3 in Figure 7

$$R^+ + \mathrm{Red} \xrightarrow{k'_{\mathrm{Red}}} R^0 + \mathrm{Ox}^+$$

The oxidized species in solution diffuses through the pores in the TiO_2 structure in the direction $x \rightarrow 0$, contributing, in principle, to the total photocurrent flow. For simplicity, the reduction of an oxidized species by a photogenerated electron, which gives rise to recombination losses,[6] is not taken into account in the model. The calculation here will be confined to illumination through the electrolyte, assuming that the thickness of the porous structure is much larger than the absorption depth of the light ($\alpha d > 1$). In this way, the contribution to the total time-resolved photocurrent flow of ions diffusing through the porous structure can be neglected with respect to the contribution of traveling electrons. This simplification is appropriate for the TiO_2 electrodes with a thickness of 0.9 and 4.0 μm illuminated via the electrolyte. Photogenerated electrons can be trapped in the surface states $R^{0/+}$, giving rise to recombination:

process 4 in Figure 7

$$e^- + R^+ \xrightarrow{\beta_R} R^0$$

The variation with time of the occupancy $f_R(x,t)$ of the states $R^{0/+}$ is given by

$$df_r(x,t)/dt = [\beta_R \Delta n(x,t) + k_{\mathrm{Red}}][1 - f_R(x,t)] - \beta_p f_R(x,t)\Delta p(x,t) \qquad (8)$$

In eq 8, the rate k_{Red} stands for the product of electrochemical rate constant k'_{Red} and the concentration of the reducing agent. Photogenerated electrons which do not recombine will travel through the porous structure toward the conducting substrate (Figure 7, process 6) due to a gradient in the quasi-Fermi level $E_{F,n}$, which is assumed to be independent of x. On their way, they can be temporarily trapped in band gap states $S^{0/+}$ (concentration s) from which they can be thermally released:

process 5 in Figure 7

$$S^+ + e^- \underset{\epsilon_S/N_C}{\overset{\beta_S}{\rightleftharpoons}} S^0$$

The variation with time of the occupancy $f_S(x,t)$ of the states $S^{0/+}$ is given by

$$df_S(x,t)/dt = \beta_S \Delta n(x,t)[1 - f_S(x,t)] - \epsilon_S f_S(x,t) \qquad (9)$$

with the thermal release rate ϵ_S of the electrons in a state located $(E_C - E_S)$ below the conduction band edge given by[19]

$$\epsilon_S = \beta_S N_C \exp[-(E_C - E_S)/k_B T] \qquad (10)$$

Instead of eq 1, valid for diffusive electron transport, the continuity equation which also accounts for trapping and recombination of the photogenerated electrons reads

$$d\Delta n(x,t)/dt = \alpha\Phi(x,t) - d\Delta j_n(x,t)/dx - s[df_S(x,t)/dt] - (\beta_R r)\,\Delta n(x,t)[1 - f_R(x,t)] \quad (11)$$

Using eqs 3, 7, 8, and 11, it can be shown that under steady state conditions

$$d\Delta j_n(x)/dx = \mu_n\epsilon[d\Delta n(x)/dx] = \alpha\Phi(x)k_{Red}/[\beta_R\Delta n(x) + k_{Red}] \quad (12)$$

If recombination can be neglected, which means $\beta_R\Delta n(x) \ll k_{Red}$, $\Delta n(x)$ can be obtained from eq 12 by integration:

$$\Delta n(x) = [\Phi(0)/\mu_n(-\epsilon)]\exp(-\alpha x) + F(\alpha d) \quad (13)$$

The integration constant $F(\alpha d)$ can, for a given thickness of the particulate electrode, be derived from appropriate boundary conditions for $x = d$. Under conditions of predominant recombination ($\beta_R\Delta n(x) \gg k_{Red}$), it is found from eq 12 that

$$\Delta n(x) = [2\Phi(0)\,k_{Red}/\mu_n(-\epsilon)\beta_R]^{1/2}\,[\exp(-\alpha x) + F(\alpha d,\beta_R,k_{Red})]^{1/2} \quad (14)$$

The integration constant $F(\alpha d,\beta_R,k_{red})$ depends on the boundary condition for $x = d$ determined by αd and the competition for surface-trapped holes between recombination and transfer to the electrolyte. From insertion of $\Delta n(x)$ into eq 4, the low-frequency limit $\Delta i_n/e\Phi(0)$ of the electron contribution to the optoelectrical admittance can be calculated as follows:

$$\Delta i_n/e\Phi(0) = [1/\Phi(0)d]\mu_n\epsilon\int_o^d \Delta n(x)\,dx = [2\mu_n(-\epsilon)k_{Red}/\Phi(0)\beta_R]^{1/2}\,[(1/d)\times \int_o^d [\exp(-\alpha x) + F(\alpha d,\beta_R,k_{Red})]^{1/2}\,dx] \quad (15)$$

If $\alpha d \gg 1$, this low-frequency limit approximates the steady state photocurrent quantum yield $\Delta i/e\Phi(0)$. The model hence predicts that for $\alpha d \gg 1$ (which is the case for the 0.9 and 4.0 μm TiO_2 electrodes) and under conditions of predominant recombination, the low-frequency limit of the optoelectrical admittance is proportional to $1/\sqrt{\Phi(0)}$, which is in agreement with the experimental results (see Figure 6, parts a and b).

In principle, the harmonically varying concentration of photogenerated electrons can be calculated using eqs 7−11. In order to obtain an analytical solution, the term $d\Delta j_n(x,\omega)/dx$ has been linearized:

$$d\Delta j_n(x,\omega)/dx = \mu_n\epsilon[d\Delta n(x,\omega)/dx] = (1/\tau_d)\Delta n(x,\omega) \quad (16)$$

In eq 16, τ_d is the transit time through the particulate electrode of electrons which are not subject to trapping/detrapping processes. It can be shown that the linearization is a reasonable simplification by inserting eq 16 into the continuity eq 1, accounting for diffusive transport only. An approximate solution for the optoelectrical admittance is then obtained (semicircle in the positive−negative quadrant with $\omega_{min} = 1/\tau_d$) which is a reasonable approximation of the exact solution (distorted semicircle with $\omega_{min} = 2.5/\tau_d$). Equation 16 was used to calculate the harmonic varying concentration of free electrons $\Delta n(x,\omega)$ when trapping/detrapping and recombination are taken into account. Insertion of $\Delta n(x,\omega)$ in eq 4 gives the optoelectrical admittance. In the frequency range $\omega > [\beta_R\Delta n(x) + k_{Red}]$, it is found that

$$\Delta i_n(\omega)/e\Phi(0,\omega) = (1/\tau_d)\int_o^d \alpha\exp(-\alpha x)\,dx\{i\omega + [i\omega(1/\tau_S)/(i\omega + \beta_S\Delta n(x) + \epsilon_S)] + (1/\tau_R) + (1/\tau_d)\}^{-1} \quad (17)$$

in which τ_R and τ_S are the lifetime of the photogenerated electrons for recombination and trapping, respectively, given by

$$1/\tau_R = \beta_R r[1 - f_R(x)] \quad (18)$$

$$1/\tau_S = \beta_S s[1 - f_S(x)] \quad (19)$$

If $\tau_S < (1/\tau_R + 1/\tau_d)^{-1}$, the calculated optoelectrical admittance corresponds to a semicircle in the positive−negative quadrant of which ω_{min} is determined by trapping and detrapping of the photogenerated electrons. If the states $S^{0/+}$ would be confined to a small energy range in the band gap, the condition $\tau_S < (1/\tau_R + 1/\tau_d)^{-1}$ would be fulfilled in that region of the porous electrode where $\beta_S\,\Delta n(x) \le \epsilon_S$. In such a case, ω_{min} would be independent or only slightly dependent on the background light intensity. However, if the states $S^{0/+}$ are distributed in energy over a range considerably exceeding k_BT, the localization time will be mainly determined by trapping in the deepest unoccupied states for which $\Delta n(x) = N_C\exp[-(E_C - E_S)/k_BT]$ (see eqs 9 and 10).[15,19] Considering the spatial dependence of $\Delta n(x)$ (eq 14), the deepest traps will be found in the region near the backcontact, where $\Delta n(x)$ is lowest (denoted as Δn_m). If the optoelectrical admittance is determined by trapping in these states, ω_{min} approximates to

$$\omega_{min} = \{[(1/\tau_R) + (1/\tau_D)]/(1/\tau_S)\}\,(2\beta_S\Delta n_m) \quad (20)$$

This means that $1/\omega_{min}$ is equal to the product of the average number of trapping events in the deepest unoccupied trapping states and the average lifetime of an electron in such a state before thermal release. From eq 14, with $x = d$, and eq 20, it follows that ω_{min} should be proportional to $\sqrt{\Phi(0)}$. First, the experimental results are considered for which it was a priori expected that mainly electrons contribute to the photocurrent flow. This is the case for the particulate electrodes of 0.9 and 4.0 μm in thickness illuminated through the electrolyte (Figure 5, parts b−e). It is indeed found that ω_{min} is proportional to $\sqrt{\Phi}$. From Figure 5, part a, it can be seen that the proportionality between ω_{min} and $\sqrt{\Phi}$ is also found for the 0.3 μm thick electrode for which $\alpha d \approx 1$. Apparently, the optoelectrical admittance mainly reflects the transport of electrons. Further investigations will be necessary to clarify why ion transport is not reflected in the optoelectrical admittance in this case. From the foregoing analysis, it can be concluded that the transport of electrons through the particulate TiO_2 electrode is limited by trapping in band gap states distributed in energy. A similar conclusion was reached in ref 15 on the basis of photocurrent transient measurements with dye-sensitized polycrystalline TiO_2 electrodes.

It might be interesting to consider the origin of the electron traps. In principle, band gap states may be related to grain boundaries or to the TiO_2/electrolyte interface. From the experimental results, it is possible to obtain a rough indication of the concentration of trapping states (see Appendix). A value in the order of 10^{17} cm^{-3} is found for the density of effective traps. From electrochemical studies,[20,21] it is known that interfacial states with a surface density of about 10^{12} cm^{-2} are active as electrochemical intermediates. When the particle size and the porosity of the TiO_2 electrodes are taken into account, it is found that a surface density of 10^{12} cm^{-2} corresponds to a volume density of 10^{17} states per cm^3 in the particulate network.

This strongly suggests that the states involved in trapping/detrapping of electrons are states present at the TiO_2/electrolyte interface. Our measurements do not provide information about the nature of the interfacial band gap states. With light absorption spectroscopy[22] and EPR measurements,[23] a Ti^{4+}/Ti^{3+} transition was observed. The predominant species involved in electron trapping probably are Ti^{4+} surface states with a distorted octahedral coordination. The levels can be distributed in energy due to surface heterogeneity and temporary fluctuations in the orientation of solvent dipoles around these states.

Our results might be important for solar cells based on dye-sensitized nanocrystalline TiO_2 electrodes. The efficiency of this type of solar cell is limited by the back transfer of electrons to the electrolyte, which is probably induced by trapping of electrons in interfacial states. Increased efficiencies might be expected if the concentration of these interfacial states is lowered or if these interfacial states are passivated.

Conclusions

It has been shown that it is possible to study the transport of photogenerated electrons through nanocrystalline TiO_2 electrodes by IMPS. A comparison of the results obtained with nanocrystalline TiO_2 electrodes and previous results with nanoporous GaP electrodes shows that recombination and trapping of photogenerated electrons play an important role in assemblies of TiO_2 particles. The model for diffusive transport, which was used for interpretation of the results with nanoporous GaP, has been extended to include recombination and trapping/detrapping processes. It was shown that electronic transport in particulate TiO_2 electrodes is limited by temporary localization of electrons in band gap states, distributed in energy. The estimated density suggests that these states are located at the TiO_2/electrolyte interface.

Appendix

As the steady state photocurrent quantum yield is in the order of 0.1, it is reasonable to assume that the electron lifetime for recombination τ_R is in the same order of magnitude as that for the transit time τ_d of free electrons through the particulate electrode, being given by $d/\mu_n|\epsilon|$. By assuming that $\tau_R \approx \tau_d$ and using eq 19 for τ_S, with $f_S = 1/2$, eq 20 becomes

$$\omega_{min} = \{[(1/\tau_R) + (1/\tau_d)]/(1/\tau_S)\}\,(2\beta_S\Delta n_m) = (8\mu_e|\epsilon|/ds)\,\Delta n_m \quad \text{(A1)}$$

Substitution of Δn_m by eq 14 (with $x = d$) shows that the proportionality factor between ω_{min} and $\sqrt{\Phi}$ is approximately given by (8/*s*) $[2\mu_n|\epsilon|k_{Red}/\beta_R]^{1/2}$. From eq 15 it follows that the proportionality factor between the steady state quantum yield and $\Phi^{-1/2}$ is approximately given by $[2\mu_n|\epsilon|k_{Red}/\beta_R]^{1/2}$. Hence, the density of traps *s* can be estimated from a comparison of both proportionality factors. This was done for the particulate electrodes of 0.9 and 4 μm in thickness using the results presented in Figures 5, parts b and c, and 6, parts a and b respectively. A value of about 10^{17} cm^{-3} for the density of effective electron traps is obtained in this way.

References and Notes

(1) Murray, C. B.; Kagan, C. R.; Bawendi, M. G. *Science* **1995**, *270*, 1335.

(2) Kagan, C. R.; Murray, C. B.; Nirmal, M.; Bawendi, M. G. *Phys. Rev. Lett.* **1996**, *76*, 1517.

(3) O'Regan, B.; Grätzel, M. *Nature* **1991**, *353*, 737.

(4) Cao, F.; Oskam, G.; Searson, P. C.; Stipkala, J. M.; Heimer, T. A.; Farzad, F.; Meyer, G. J. *J. Phys. Chem.* **1995**, *99*, 11974.

(5) Hodes, G.; Howell, I. D.; Peter, L. M.; *J. Electrochem. Soc.* **1992**, *139*, 3136.

(6) Södergren, S.; Hagfeldt, A.; Olsson, J.; Lindquist, S.-E. *J. Phys. Chem.* **1994**, *98*, 5552.

(7) Hotchandani, S.; Kamat, P. V. *J. Electrochem. Soc.* **1992**, *139*, 1630.

(8) Hoyer, P.; Weller, H. *J. Phys. Chem.* **1995**, *99*, 14096.

(9) de Jongh, P. E.; Vanmaekelbergh, D. *Phys. Rev. Lett.* **1996**, *77*, 3427.

(10) Granqvist, C. G. *Solid State Ionics* **1992**, *53*−*56*, 479.

(11) Erné, B. H.; Vanmaekelbergh, D.; Kelly, J. J. *Adv. Mater.* **1995**, *7*, 739.

(12) Erné, B. H.; Vanmaekelbergh, D.; Kelly, J. J. *J. Electrochem. Soc.* **1996**, *143*, 305.

(13) Iranzo Marín, F.; Hamstra, M. A.; Vanmaekelbergh, D. *J. Electrochem. Soc.* **1996**, *143*, 305.

(14) Vanmaekelbergh, D.; Iranzo Marín, F.; van de Lagemaat, J. *Ber. Bunsen-Ges. Phys. Chem.* **1996**, *100*, 616.

(15) Schwarzburg, K.; Willig, F. *Appl. Phys. Lett.* **1991**, *58*, 2520.

(16) Tributsch, H.; Willig, F. *Sol. Energy Mater. Sol. Cells* **1995**, *38*, 355.

(17) Wahl, A.; Carroy, A.; Jermann, B.; Dolata, M.; Kedzierzawski, P.; Chatelain, C.; Monnier, A.; Augustynski, J. *J. Electroanal. Chem.* **1995**, *396*, 41.

(18) Henglein, A. *Top. in Curr. Chem.* **1988**, *143*, 115.

(19) Simmons, J. G.; Taylor, G. W. *Phys. Rev. B* **1971**, *4*, 502.

(20) Kobayashi, K.; Aikawa, Y.; Sukigara, M. *J. Appl. Phys.* **1983**, *54*, 2526.

(21) Vandermolen, J.; Gomes, W. P.; Cardon, F. *J. Electrochem. Soc.* **1980**, *127*, 324.

(22) Bahnemann, D.; Henglein, A.; Lilie, J.; Spanhel, L. *J. Phys.Chem.* **1984**, *88*, 709.

(23) Howe. R. F.; Grätzel, M. *J. Phys. Chem.* **1985**, *89*, 4495.